The Search for Lunar Present-day Tectonic Activity using LO and LRO Images V. T. Bickel[1,2] and A. Valantinas[3], [1]Max Planck Institute for Solar System Research, Goettingen, Germany (bickel@mps.mpg.de), [2]ETH Zurich, Zurich, Switzerland, [3]University of Bern, Bern, Switzerland.

Introduction: Pre-Apollo and Apollo-era orbital observations revealed local, geomorphologic evidence for recent and potentially ongoing tectonic activity associated with wrinkle ridges [1] and lobate scarps [2]. The global distribution and extent of this activity could not be determined, however, due to limitations of the data. More recent studies examined newly acquired datasets and observed additional, geomorphologic evidence for tectonic activity, such as exposed, fresh boulder fields on top of wrinkle ridges in the lunar nearside maria [3] and morphologically crisp lobate scarps, primarily found in the lunar highlands [4, 5]. The Apollo seismometers recorded shallow and deep moonquakes, which may be echoes of such tectonic activity [6]. However, more evidence is required to link orbital, global observations to the recorded seismic data: there are no direct observations of present-day co-seismic surface changes and displacements yet. Further, the rate and scale of wrinkle ridge and lobate scarp activity remains unclear.

Here, we attempt to directly observe and characterize potential present-day surface displacements and changes associated with lobate scarp and wrinkles ridge activity by cross-correlating pre-Apollo Lunar Orbiter V (LO) and modern Lunar Reconnaissance Orbiter (LRO) NAC images. The fusion of both datasets allows for high-resolution change detection with the longest possible temporal baseline.

Data: We use a total of 8 map-projected and orthorectified image pairs to investigate 6 sites of interest, 4 with wrinkle ridges and 2 with lobate scarps, specifically: 3 LO-LRO image pairs for the Marius Hills and Dorsa Aldrovandi sites; 2 LRO-LRO pairs for the Sulpicius Gallus and Flamsteed sites, which also act as control sites due to the excellent affinity of the respective image pairs; and 3 LRO-LRO pairs for the Arnold-A and Vitello sites. Due to the severe scarcity of LO data, we were only able to identify two sites of interest that offer the full temporal baseline (LO-LRO). The selection of sites is additionally limited by the quality (viewing geometry, illumination conditions, spatial resolution, artifacts) of the LO data; noteworthy LO artifacts are coffee ring patterns (read-out noise), reseaus, stitch marks, and framelet shifts. Therefore, we selected additional LRO-LRO pairs to cover a larger number of interesting sites. A list with detailed information about the sites of interest and the imagery used is shown in Table 1.

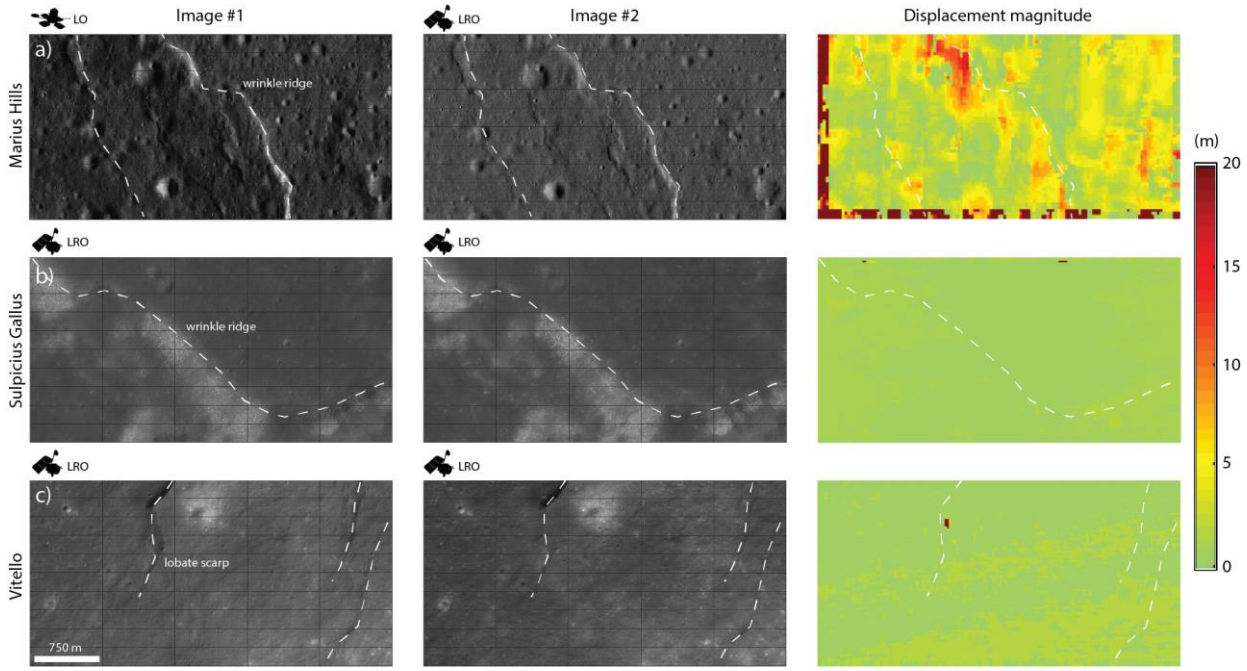

Figure 1. Image pairs and displacement fields derived for three exemplary sites with either wrinkle ridges or lobate scarps, using LO–LRO and LRO–LRO pairs (as indicated). The apparent displacement in the Marius Hills site is caused by LO image geometry issues in combination with local topography and framelet shifts. Raw LROC image credits to LROC/GSFC/ASU.

Digital Image Correlation: We use a digital image correlation (DIC) algorithm called "DIC FFT" [7] (Fast Fourier Transform-based, freely available here: https://github.com/bickelmps/DIC_FFT_ETHZ) (MIT Licence) to co-register and scan all image pairs for surface changes. This algorithm is able to pick up sub-pixel-scale surface displacements that occurred between the acquisitions of image #1 and #2, i.e., is theoretically able to detect surface movements on the order of <<1 m, if present. We point out that image correlation algorithms are highly sensitive to image artifacts, illumination, and geometry that can mimic true change, such as present in LO data.

Results and Discussion:

We note that the artifacts associated with LO imagery cause noise in the derived displacement maps (see Figure 1a). Most importantly, the variable geometric stability of the LO imagery (e.g. framelet shifts) emulates displacements, particularly in locations with distinct topographic relief. We do not expect that the observed noise would overprint or eliminate the signature of true, continuous, and large-scale tectonic surface displacement, as the distribution of noise is localized, heterogeneous and interlaced with non-affected regions without any displacements. In addition, the results derived in our validation sites indicate that the used image products as well as the algorithm are not affected by systematic errors and thus produce reliable displacement maps (see Figure 1b).

The DIC algorithm does not pick up surface displacements or changes in any of the selected sites of interest (e.g. see Figure 1c) and a visual investigation of all image pairs does not result in any detection of activity. A manual investigation of an additional lobate scarp in Mare Serenitatis (22.26°N,29.1°E) using a pair of low-quality LO images (5066HR & 5068HR, no DIC possible) does not yield any observable changes either.

The fact that we were not able to observe present-day surface changes in 5 wrinkle ridge and 3 lobate scarp sites could be interpreted in two different ways: For example, the ongoing displacements and changes could be below the algorithm's sensitivity threshold, which depends on resolution and temporal baseline. Within lunar geologic timescales surface changes might need more than ~50 years to be observable from orbit. This would suggest that lunar tectonic displacement velocities along wrinkle ridges and lobate scarps are below ~0.03 to ~0.7 m/a, on average. Alternatively, our results might indicate that tectonic activity is episodic and more data is needed to analyze additional sites of interest. As LRO continues to map the lunar surface, a) more appropriate image pairs with b) longer temporal baselines become available to search for present-day surface changes in other potentially active regions of the Moon.

References: [1] Schultz, P. H. (1976), *Moon Morphology* [2] Binder, A.B. & Gunga, H.C. (1985), *Icarus, 63.* [3] Valantinas, A. & Schultz, P.H. (2020), *Geology, 48.* [4] Watters, T.R. et al., (2010), *Science, 329.* [5] Watters, T.R. et al., (2019) *Nature Geo.*, 12. [6] Nakamura, Y. et al., (1982), *JGR, 87.* [7] Bickel, V.T. et al., (2018) *Remote Sens. (10).*

Site	Type	LAT	LON	Image pair	R (m/pix)	Δt (a)	ΔE (°)	v (m/a)
Sulpicius Gallus*	W	21.60°N	11.36°E	M1241241067LC M1167091987RC	~1.6	~5.5	~0.57	~0.29
Flamsteed*	W	3.63°S	48.71°W	M1185143612RC M193274942RC	~2.1	~3	~0.01	~0.7
Dorsa Aldrovandi	W	22.70°N	28.85°E	5069HR M1234067630LC	~1.25	~49	~0.86	~0.03
Marius Hills #1	W	14.03°N	56.26°W	5214HR M1108646684LC	~1.25	~45	~9.1	~0.03
Marius Hills #2	W	14.38°N	56.42°W	5215HR M1108646684RE	~1.25	~45	~9.1	~0.03
Arnold-A	L	71.26°N	36.07°E	M157365463LC M155004439LC	~1	~0.1	~0.01	~10
Vitello #1	L	39.95°S	40.63°W	M183788674RC M1116783877LC	~0.7	~1.1	~0.55	~0.64
Vitello #2	L	34.46°S	37.92°W	M107122037LC M1239193382RC	~0.78	~8.5	~0.55	~0.09

Table 1. List of all sites of interest and images used, including type (W = wrinkle ridge, L = lobate scarp), spatial resolution (R), temporal baseline (Δt), emission angle difference (ΔE), and estimated maximum, average displacement velocity (v); *denotes validation sites. The Mare Serenitatis site is not listed, as it has only been used for a visual analysis.